Optically pumped intersubband laser: Resonance positions and many-body effects

H. C. Liu*
Institute for Microstructural Sciences, National Research Council, Ottawa, Ontario, Canada K1A 0R6

A. J. SpringThorpe
Nortel Microelectronics, Nortel Networks, Ottawa, Ontario, Canada K2H 8E9

(Received 6 December 1999; revised manuscript received 9 February 2000)

Intersubband transition (IT) between confined states in quantum wells (QW's) is a fully collective phenomenon displaying distinct many-body effects. These effects are seen in an optically pumped ITQW laser. The strong pump, needed to achieve population inversion, ''undresses'' the depolarization effect, leading to a redshift in the absorption peak position. The emission wavelength is also redshifted due to a combination of Hartree, exchange-correlation, and depolarization effects. The depolarization shift is in the opposite direction for the emission between population inverted levels than for the usual absorption case.

The dream of making a quantum well (QW) laser[1,2] based on intersubband transition (IT) was first realized by Faist *et al.*[3] The quantum cascade laser[3,4] is an electrically pumped device. Although electrical injection is desirable for most applications, optical pumping may provide some performance advantages and could be useful in certain applications. Optically pumped ITQW lasers have been recently demonstrated,[5,6] which were termed quantum fountain lasers. Theoretical analyses of the performance and optimization have been performed.[7,8] Work is also underway on optically pumped lasers covering the far-infrared region.[9,10]

This paper reports on spectroscopic results of IT absorption resonances and pumping and lasing positions. Clear differences between the positions of low-power absorption resonances and the high-power pumping and the resulting lasing positions are seen. The importance of including many-body effects is demonstrated. It is shown that all many body effects (Hartree, exchange correction, and depolarization) should be considered to account for the observed results. It is also noted that the depolarization shift is in the opposite direction for emission in a population inverted system than in the usual equilibrium case.

The sample used here is similar to that designed and studied by Gauthier-Lafaye *et al.*[6] with an important difference: The substrate here is undoped (insulating), which makes transmission/absorption measurements easy. The active region consists of 150 repeats of coupled double QW of 8.2-nm GaAs, 1.2-nm $Al_{0.35}Ga_{0.65}As$, and 5.3-nm GaAs. The separation between periods is a 20.7-nm $Al_{0.35}Ga_{0.65}As$ barrier with its center Si-δ-doped to 3×10^{11} cm^{-2}. Every period (i.e., the double well) is then populated with 3×10^{11} cm^{-2} electrons. The total multiquantum well (MQW) thickness is therefore 5.33 μm. The waveguide layers are (starting from the substrate) 5.2-μm $Al_{0.87}Ga_{0.13}As$, 0.78-μm GaAs, 5.33-μm MQW, and 1.81-μm GaAs. The waveguide confines TM_0 modes for both 9- and 15-μm wavelengths. The structural parameters have been confirmed by x-ray and transmission electron microscopic measurements. A schematic of the double-well structure is shown in Fig. 1. The double well confines four bound states: E_1, E_2, E_3, and E_4. The highest level (E_4) plays no role in this device. The three-level laser works by pumping from E_1 to E_3 and emitting from E_3 to E_2. The separation between E_1 and E_2 is close to (but larger than) the GaAs longitudinal optical-phonon energy to facilitate a rapid relaxation of electrons from E_2 to E_1.

For the emission measurement, a pulse CO_2 laser (Edingburgh Instruments MTL-3GT) was used for pumping. The laser delivers up to 40 mJ per pulse with a width of 50 ns. The laser beam (about 6 mm in diameter) was focused using a 3-in. focal length antireflection coated ZnSe cylindrical lens. A sample 3 mm long at 80 K was pumped by the edge as in Refs. 5 and 6. The experimental geometry is schematically shown in the left inset to Fig. 1. The maximum power

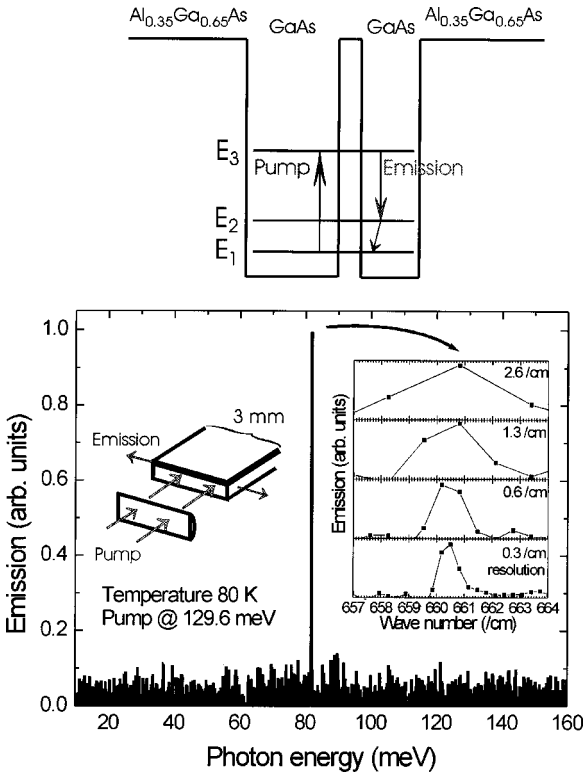

FIG. 1. Top: schematic quantum well structure, and bottom: emission spectrum. The left inset depicts the pump and emission optical layout; and the right shows the emission spectra on an expanded scale, taken with different spectrometer resolutions. The pump intensity is about 50% above the threshold.

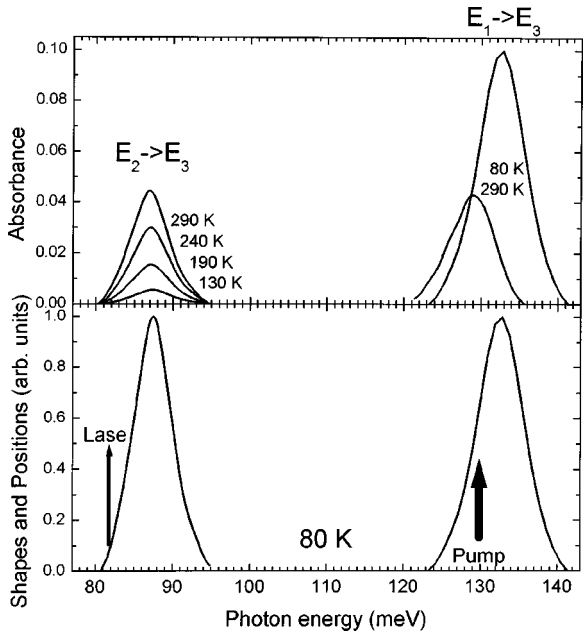

FIG. 2. Top: absorption spectra at different temperatures, and bottom: 80 K absorption spectral shapes and pumping and lasing positions. The incident light is at the Brewster angle (73°) and is *p* polarized. In the bottom part, solid curve shows the normalized 80 K $E_1 \rightarrow E_3$ absorbance, and the dashed curve gives the $E_2 \rightarrow E_3$ absorption line shape extrapolated from the corresponding curves from the top part to 80 K.

that can be put on the sample is limited by the surface damage threshold of GaAs, which is about 100 kW peak power for the laser pulses used here. The focal spot is estimated to be 6×0.150 mm^2, which implies that the maximum input power density is about 10 MW/cm^2. The lasing spectra were collected using a Bomem DA8 Fourier-transform interferometer with a HgCdTe detector and an event-locking accessory (Zaubertek ELFS40). A typical emission spectrum is shown in Fig. 1. The right inset shows the emission peak on an expanded scale at several spectrometer resolutions.

The important results are shown in Fig. 2 where the absorption spectra at different temperatures are graphed. IT absorption from E_1 to E_3 is clearly visible, centered at 129 meV (9.6 μm) at room temperature (290 K) and 132.6 meV (9.3 μm) at 80 K. Because of the thermally populated electrons on E_2 subband at higher temperatures (>100 K), a feature due to E_2 to E_3 transition is seen at about 87 meV, which disappears at 80 K and displays nearly no shift. It is important to note that the resonance linewidths are quite narrow. The full width at half maximum for the E_1 to E_3 transition at 80 K is only 7 meV (5% of the transition energy). This implies that the period-to-period uniformity of the 150 period MQW structure is very good. This results in a narrow gain spectrum and single longitudinal lasing mode (see Fig. 1) for pump powers not too high above the threshold. This is in contrast to Refs. 5 and 6 where a multimode emission with about five peaks was observed. Within the range of the input power (2–10 MW/cm^2) of our experiment our laser operated only on a single mode. To make certain that the emission is single mode, we collected spectra at various spectrometer resolutions from 2.6–0.3 cm^{-1}. Only a single peak (progressively narrowed with increasing resolution shown in the right inset to Fig. 1) was observed. Note that the expected longitudinal mode separation is about 0.5 cm^{-1} for a 3-mm-long cavity.

The most interesting feature in Fig. 2 is that the pump position (130 meV) does not coincide with the peak of the E_1 to E_3 absorption (132.6 meV) and that the lasing position (81.8 meV) is also redshifted from the peak of the E_2 to E_3 absorption (87.3 meV). We varied the CO_2 laser wavelength within the 9P (9.6 μm) branch (129−131 meV) and observed no appreciable change. This rules out the possible emission origin from a resonant Raman process. When the laser was tuned to the 9R (9.3 μm) branch (133-134 meV), though nearly exactly matched to the absorption peak, no lasing was observed. Note that the shifts that we are discussing are quite small in absolute values (1.6–3.6 meV for the pump and 5.5 meV for the emission), but clearly observable (see Fig. 2) due to the narrow absorption linewidths. Since the samples used for absorption and lasing measurements are not the same piece of the wafer, we must rule out any possible effects due to wafer nonuniformity. We have carefully checked the wafer uniformity by measuring a stripe across the 3-in. diameter of the wafer. For this study, we only used the material from the center part of the 2-in. in diameter, where the wafer is uniform within the accuracies of all our characterization techniques. We will show that the shifts are accounted for by many-body and collective effects.

To explain the redshift in E_1 to E_3 pump position, we realize that the input pump power is above the saturation intensity[11] $I_0 \propto \Gamma_1 \Gamma_2 / |z_{13}|^2$ where Γ_2 half-linewidth (related to dephasing time $T_2 = \hbar/\Gamma_2$), Γ_1 homogeneous half-width (related to lifetime $T_1 = \hbar/\Gamma_1$), and z_{13} dipole matrix between state 1 and 3. The value of I_0 for the E_1 to E_3 transition is about 1 MW/cm^2. For pump intensity $I > I_0$, the absorption peak redshifts towards the position as if the depolarization effect is eliminated, so called ''undressing'' demonstrated recently.[12,11] The depolarization energy is calculated by the well-known expression[13,11]

$$\Delta E_{depol,13} \approx \frac{e^2 n_{2D}}{\epsilon} S_{13}, \tag{1}$$

where n_{2D} is the two-dimensional electron density, ϵ is the dielectric constant multiplied by the vacuum permitivity, and the depolarization integral is

$$S_{13} = \int_{-\infty}^{\infty} dz \left| \int_{-\infty}^{z} dz' \psi_3(z') \psi_1(z') \right|^2. \tag{2}$$

The value of $\Delta E_{depol,13}$ is evaluated to be 2.2 meV. This is in reasonable agreement with the observed redshift from 1.6 meV (absorption peak position–pump position $= 132.6 - 131$ meV) to 3.6 meV ($132.6 - 129$ meV). The shift is therefore attributed to the undressing of the collective depolarization effect by a strong pump.[12] This undressing effect can be seen clearly by reproducing the calculation of Załużny[11] shown in Fig. 3 using parameters appropriate for the E_1 to E_3 transition in our structure. It is seen that as the pumping intensity is increased the absorption peak shifts to lower energy. We also plot the density difference between the E_1 and E_3 subbands (normalized to low-pumping value). It is seen that as the pumping is increased the electron densities on the E_1 and E_3 subbands become nearly equal.

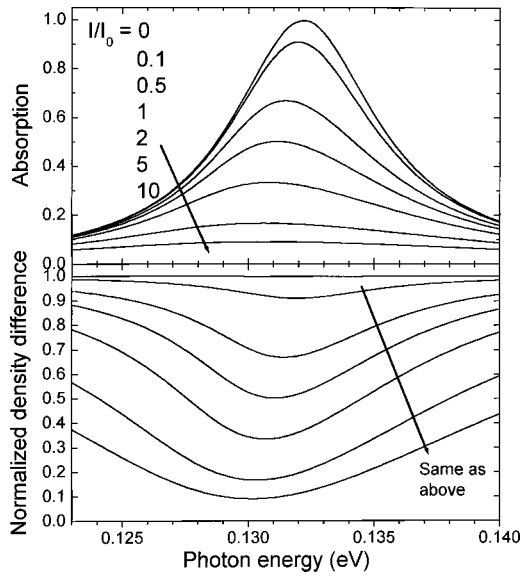

FIG. 3. Top: calculated absorption spectra for different pumping intensities (I). The saturation intensity is I_0. The curves are normalized with respect to the lower power ($I=0$) spectrum. Bottom: normalized density differences for different pumping intensities. If $n_1(I)$ and $n_3(I)$ are electron densities on E_1 and E_3 subbands, respectively, the plotted quantity is $[n_1(I)-n_3(I)]/n_1(I=0)$.

To understand the shift in the lasing wavelength with respect to the E_2 to E_3 absorption peak position, we note that as the pump intensity is increased, the population on E_3 increases until at and beyond saturation where the populations on E_1 and E_3 become approximately equal (see lower part of Fig. 3). At the same time, the population on E_2 remains small, determined by the relaxation times from E_3 to E_2 (τ_{32}) and E_2 to E_1 (τ_{21}). We therefore consider the effect of this charge redistribution on the positions of subband E_2 and E_3. Specifically the shifts in E_2 and E_3 caused by their populations (Hartree and exchange correlation) and the depolarization involved in the E_3 to E_2 emission are estimated.

For simplicity, we consider the various effects one by one in the leading order perturbation. Let $\psi_i(z)$ be the wave function for the E_i state, then the Hartree correction for level i is (by first order perturbation theory)

$$\Delta E_{H,i}=(-e^2/\epsilon)\int_{-\infty}^{\infty}dz|\psi_i(z)|^2\int_{-\infty}^{z}dz'(z-z')\Delta N(z'), \tag{3}$$

where the superscript (0) represents the quantity at zero pumping, $\Delta N=N-N^{(0)}$, the three-dimensional density

$$N(z)=\sum_i n_i|\psi_i(z)|^2, \tag{4}$$

and n_i is the two-dimensional density on the E_i subband.

For the calculation of exchange correlation, we use the local-density approximation (LDA) and calculate the shift similarly to the above:

$$\Delta E_{xc,i}=\int_{-\infty}^{\infty}dz|\psi_i(z)|^2[V_{xc}(n_i)-V_{xc}(n_i^{(0)})], \tag{5}$$

where the LDA potential is

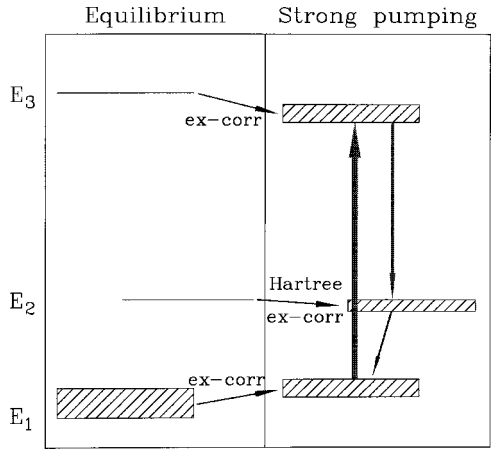

FIG. 4. Schematic illustration of level shifts. The left part shows the level positions (E_1, E_2, and E_3) in equilibrium at low temperature. The hatching indicates electron population. The right part shows the situation under a strong pump between E_1 and E_3. Due to the population redistribution, the main causes of the shifts in subband positions are labelled. The exchange-correction (ex-corr) effect shifts E_3 downward and E_1 upward; while Hartree and ex-corr shifts are in opposite directions for E_2. The Hartree contribution to E_1 and E_3 is small.

$$V_{xc}=-\frac{0.916}{r_s}+0.062182\ln r_s-0.093288 +0.01328 r_s\ln r_s-0.02046 r_s, \tag{6}$$

where $r_s=1/(4\pi a^3 n(z)/3)^{1/3}$, $n(z)=n_i|\psi_i(z)|^2$, a is the effective Bohr radius (≈ 10 nm for GaAs conduction band), and the energy unit is in the effective Rydberg (≈ 6 meV). We have used an improved form of the LDA potential given in Perdew and Wang,[14] not the early form by Hedin and Lundqvist.[15]

When the pump intensity is sufficiently high ($I>I_0$), we have $n_1\approx n_3$. The relative densities between E_3 and E_2 are determined by $n_3/\tau_{32}=n_2/\tau_{21}$. The relaxation times are taken to be $\tau_{21}\approx 0.5$ ps and $\tau_{32}\approx 1.5$ ps,[5,7] i.e., $\tau_{32}/\tau_{21}=3$ and $n_3=3n_2$. In this case, we have $n_1=n_3=(3/7)n_{2D}$ and $n_2=(1/7)n_{2D}$, where $n_{2D}=3\times 10^{11}$ cm^{-2} is the total electron density per double well. Using these values and Eqs. (3) and (5), the Hartree effect causes a net redshift of 1.6 meV, the exchange correlation gives a net redshift of 1.6 meV. The Hartree shift mainly comes from the upshift of the E_2 state; whereas the exchange-correlation shift comes from the down shift of E_3 level. These effects are schematically shown in Fig. 4. In addition, in an inverted system the depolarization causes a redshift[16] instead of the blueshift in the usual case. The magnitude is given by Eq. (1) with n_{2D} replaced by the population difference (n_3-n_2) and S_{13} by S_{32}. The value is found to be 1.1 meV. Adding all contributions (1.6+1.6 +1.1 meV), we get a calculated redshift of 4.3 meV, compared with the observed 5.5 meV. The agreement is acceptable given the simplicity of the theoretical model.

We now comment on other possible interpretations of our results. Given the high-pump input power, the effective electron temperature could be much higher than the heat sink. Simulations of Wang *et al.*[8] predicted substantially higher electron temperatures under strong pumping, especially for

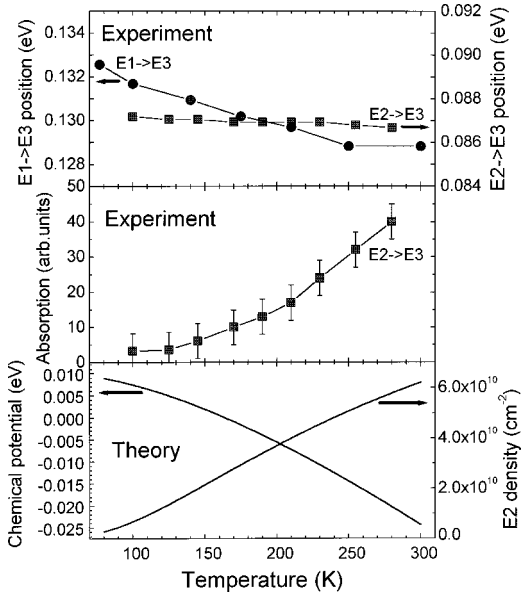

FIG. 5. Top: Resonance positions, middle: integrated E_2 to E_3 absorption, and bottom: calculated chemical potential and electron density on E_2 subband, all versus temperature. The energy reference for the chemical potential is at E_1 level.

the E_2 subband. This raises an obvious possibility, i.e., the observed shifts could be due to an increase in temperature. As shown in Fig. 5 (top), a temperature increase does cause a red shift in the E_1 to E_3 transition, however, the E_2 to E_3 position is practically robust versus temperature. This suggests that the temperature rise is not the cause. Note that this argument is not rigorous because a change in lattice or electron temperature may not lead to the same result. Note also that our sample behaves differently from that reported by Lavon *et al.*[17] where both E_1 to E_3 and E_2 to E_3 transitions showed redshifts with increasing temperature. The possible high-electron temperature raises another possibility: due to band nonparabolicity, intersubband resonance should display a redshift for electrons with high in-plane momenta. This mechanism is not ruled out.

Figure 5 also shows other relevant results. The integrated E_2 to E_3 absorption shown in the middle part is expected to be proportional to the E_2 density (see the bottom part for comparison). We point out that the chemical potential changes substantially with temperature (bottom part in Fig. 5). The standard approximation of using a fixed chemical potential (Fermi energy) is only valid at low temperatures (<80 K). Knowing the resonance positions $E_3-E_1=133$ and $E_3-E_2=87$ meV and the chemical potential of 9 meV at 80 K, the energy separation between the top of the Fermi sea and E_2 is $133-87-9=37$ meV, which is slightly larger than the phonon energy.

To conclude, we have presented a study on the resonance positions in an optically pumped ITQW laser. Comparing absorption resonance positions and lasing and pumping energies, clear shifts are observed and attributed to many-body effects. We compare experimental results with calculations including Hartree, exchange-correlation, and depolarization effects. We must point out that our calculation is not fully self-consistent: We analyzed the pump transition as though we had a two-level system. We then inferred a density distribution of electrons among the three levels and calculated the expected emission energy. A self-consistent simulation could employ a density matrix formalism for a three-level system. Clearly more rigorous theoretical work is needed. Finally, with the unoptimized sample (which lases only at high-pumping intensities), we cannot completely rule out other possible effects that could also cause shifts between absorption and gain spectra.[18] Clearly, more experimental work is also needed.

We thank G. C. Aers and A. Delage for quantum-well and wave-guide simulations, E. Dupont, C. Dharma-wardana, P. Hawrylak, F. Julien, and M. Załużny for discussions, M. Gao for sample preparation, J. McCaferry for TEM measurements, and A. Shen for x-ray measurements.

*FAX: 613 990 0202. Electronic address: h.c.liu@nrc.ca

[1] R.F. Kazarinov and R.A. Suris, Fiz. Tekh. Poluprovodn. **5**, 797 (1971) [Sov. Phys. Semicond. **5**, 707 (1971)].

[2] H.C. Liu, J. Appl. Phys. **63**, 2856 (1988); **69**, 2749 (1991).

[3] J. Faist, F. Capasso, D.L. Sivco, C. Sirtori, A.L. Hutchinson, and A.Y. Cho, Science **264**, 553 (1994).

[4] J. Faist, F. Capasso, C. Sirtori, D.L. Sivco, and A.Y. Cho, in *Intersubband Transition in Quantum Wells: Physics and Device Applications*, Vol. 67 of *Semiconductors and Semimetals*, edited by H. C. Liu and F. Capasso (Academic, San Diego, 2000), Chap. 1.

[5] O. Gauthier-Lafaye, P. Boucaud, F.H. Julien, S. Sauvage, J.M. Lourtioz, V. Thierry-Mieg, and R. Planel, Appl. Phys. Lett. **71**, 3619 (1997).

[6] O. Gauthier-Lafaye, F.H. Julien, S. Cabaret, J.M. Lourtioz, G. Strasser, E. Gornik, M. Helm, and P. Bois, Appl. Phys. Lett. **74**, 1537 (1999).

[7] J. Wang, J.-P. Leburton, Z. Moussa, F.H. Julien, and A. Sa'ar, J. Appl. Phys. **80**, 1970 (1996).

[8] J. Wang, J.-P. Leburton, F.H. Julien, and A. Sa'ar, IEEE Photonics Technol. Lett. **8**, 1001 (1996).

[9] I. Lyubomirsky and Q. Hu, Appl. Phys. Lett. **73**, 300 (1998); see also a comment by M. Dutta and M.A. Stroscio, *ibid.* **74**, 2555 (1999); and the reply by I. Lyubomirsky and Q. Hu, *ibid.* **74**, 3065 (1999).

[10] I. Lyubomirsky, Q. Hu, and M.R. Melloch, Appl. Phys. Lett. **73**, 3043 (1998).

[11] M. Załużny, Phys. Rev. B **47**, 3995 (1993).

[12] K. Craig, B. Galdrikian, J.N. Heyman, A.G. Markelz, J.B. Williams, M.S. Sherwin, K. Campman, P.F. Hopkins, and A.C. Gossard, Phys. Rev. Lett. **76**, 2382 (1996).

[13] S.J. Allen, D.C. Tsui, and B. Vinter, Solid State Commun. **20**, 425 (1976).

[14] J.P. Perdew and Y. Wang, Phys. Rev. B **45**, 13 244 (1992).

[15] L. Hedin and B.I. Lundqvist, J. Phys. C **4**, 2064 (1971).

[16] M.V. Kisin, M.A. Stroscio, G. Belenky, and S. Luryi, Appl. Phys. Lett. **73**, 2075 (1998).

[17] Y. Lavon, A. Sa'ar, J. Wang, J.-P. Leburton, F.H. Julien, and R. Planel, Appl. Phys. Lett. **69**, 197 (1996).

[18] M.V. Kisin, V.B. Gorfinkel, M.A. Stroscio, G. Belenky, and S. Luryi, J. Appl. Phys. **82**, 2031 (1997).